region of the northern plains is a 3,300-km impact basin, a feature so large that it must date from the early heavy bombardment. That hypothesis was strengthened by the discovery of a broad depression, the outline of which coincides with that of the buried basin[4], and by a large, positive, gravity anomaly having a magnitude consistent with the nearly complete infilling of an ancient impact depression by younger sedimentary and volcanic material[5]. But the work of Frey *et al.* extends the mapped area of ancient surface to nearly the entire northern lowlands and quantifies the density of impact features.

The crustal dichotomy, then, might be the most ancient structural feature preserved on the Martian surface. If so, there are several implications for our understanding of the geological and geophysical evolution of the planet. The northern lowlands must have exerted a primary influence on the flow direction of surface and subsurface water on Mars for the entire duration of preserved geological history[6], and much of the material making up the veneer overlying the ancient northern surface probably consists of sediments. The high density of newly detected large impact structures within the Utopia basin — whose original depth might have been comparable to the nearly 10-km relief of Hellas, a partly filled basin of similar diameter in the south — implies that much of the resurfacing of the northern hemisphere occurred during the period of early impact bombardment. The incomplete burial of impact craters allows the thickness of the younger northern-plains units to be estimated at typically 1–2 km, but that figure could exceed 5 km in a few areas near major volcanic centres where no older craters can be seen[2]. The difference in elevation between the north and the south requires a generally thinner crust in the north[5]. Because lateral flow of lower crust would tend to reduce such variations if the temperature at the base of the crust exceeded about half the local melting temperature[5,7], preservation of the dichotomy implies that the lower crust cooled rapidly after early crustal formation — perhaps as a result of deep hydrothermal circulation[8].

A question, first raised when the crustal dichotomy was discovered, remains. What caused it? Suggestions have ranged from removal of crust in the northern hemisphere by one or more large impacts, to hemispherical differences in crustal addition or internal recycling by dynamical processes in the underlying mantle. None has proved fully persuasive[9]. At the least, however, the demonstration that the crust in both hemispheres formed very early in the history of Mars adds a fresh requirement for any successful explanation of this long-standing mystery. ■

Sean C. Solomon is in the Department of Terrestrial Magnetism, Carnegie Institution of Washington, Washington, DC 20015, USA.
e-mail: scs@dtm.ciw.edu

1. Smith, D. E. *et al. J. Geophys. Res.* **106,** 23689–23722 (2001).
2. Frey, H. V., Roark, J. H., Shockey, K. M., Frey, E. L. & Sakimoto, S. E. H. *Geophys. Res. Lett.* **29,** 10.1029/2001GL013832 (2002).
3. McGill, G. E. *J. Geophys. Res.* **94,** 2753–2759 (1989).
4. Smith, D. E. *et al. Science* **284,** 1495–1503 (1999).
5. Zuber, M. T. *et al. Science* **287,** 1788–1793 (2000).
6. Baker, V. R. *Nature* **412,** 228–236 (2001).
7. Nimmo, F. & Stevenson, D. J. *J. Geophys. Res.* **106,** 5085–5098 (2001).
8. Parmentier, E. M. & Zuber, M. T. *Lunar Planet. Sci.* **33,** 1737 (2002).
9. McGill, G. E. & Squyres, S. W. *Icarus* **93,** 386–393 (1991).

Embryology

Fluid flow and broken symmetry

Claudio D. Stern

The asymmetries between the right- and left-hand sides of the body are initiated at an early stage of development. Two groups provide welcome news of progress in revealing the mechanism concerned and its generality.

How an embryo first distinguishes its left from its right side has baffled embryologists for a long time. The rotational beating of cilia — hair-like structures attached to individual cells — is known to be essential for the process. But cilia have been seen only in mouse embryos, and it has remained unclear whether their movement could really generate the necessary molecular asymmetries. Papers by Essner *et al.*[1] and Nonaka *et al.*[2] (pages 37 and 96 of this issue) set our understanding on a much firmer footing in both respects.

Despite its superficial appearance of bilateral symmetry, the vertebrate body plan is asymmetric in several respects, most obviously in the position of internal organs such as the heart and parts of the gut. Left–right asymmetry first arises in the embryo at around the stage — the gastrula — when the three major cell layers of ectoderm, mesoderm and endoderm are first laid down. But until recently we knew virtually nothing about the molecular mechanisms responsible.

The turning point came in 1995 when four genes (*Sonic hedgehog*, *Nodal*, *HNF3β* and the *Activin-receptor IIA*) were identified as being expressed on one or the other side of the chick embryo at the gastrula stage, and their activities were implicated in heart turning[3]. However, subsequent work revealed that only one of these, *Nodal*, is expressed asymmetrically in all vertebrates. Shortly afterwards it was discovered that a mouse mutant, called *iv* and characterized by random positioning of internal organs, carries a mutation that inactivates left–right dynein (LRD), a protein required for the beating of cilia[4]. Researchers then looked for cilia in the mouse gastrula and found that the 'node', a critical organizing structure in the midline of the early embryo, does indeed possess short cilia protruding from its cells, which beat in an anticlockwise circular motion and generate a leftwards flow of fluid that is strong enough to displace solid particles to the left[5,6]. But again, the cilia could be found only in the mouse. Could different vertebrates have evolved different ways of establishing asymmetry? And could the beating of cilia really be sufficient to generate molecular asymmetry by removing a 'morphogen' signal from one side of the embryo and enriching it on the other?

The papers by Essner *et al.*[1] and Nonaka *et al.*[2] answer both questions. Essner *et al.* reveal that cilia, as well as LRD, are indeed present in all the major vertebrate groups at appropriate stages and locations to generate left–right asymmetry. Nonaka *et al.* show that a flow of fluid in the reverse direction to that generated by cilia can randomize embryonic asymmetry — and that artificially induced fluid flow is enough to control the position of the internal organs in *iv* mutant mice.

The idea that the circular beating of tiny cilia could be enough to generate a biologically meaningful molecular gradient within a large, relatively open fluid space seemed rather unlikely when it was first proposed[5]. Nonaka and colleagues have designed an ingenious mechanical device to demonstrate that it is indeed possible to control the distribution of molecules by regulating the direction of fluid flow around embryonic cells. The experimental design was similar to one described nearly 20 years ago[7]. There, it was demonstrated that gentle flow applied to a wounded sheet of cells in culture restricted healing growth of the wound to the downstream side of the flow, as if it were controlled by the local distribution of a growth factor. The study by Nonaka *et al.* now reveals a likely role for this mechanism *in vivo*. It highlights the significance of biomechanical phenomena in generating biological pattern, an idea that has hitherto been broadly dismissed.

In contrast, the finding[1] that cilia and LRD are associated with the node or its equivalent structures in all major vertebrate groups is reassuring. Developmental biologists generally choose one 'model' organism or another according to the experimental advantages it offers, with the underlying assumption that the basic principles should

be much the same in different species. That this is generally true is evident in a huge body of data revealing that genes responsible for patterning the body of the fruitfly have similar functions in vertebrates.

Several questions remain open. What, for instance, are the critical molecules whose distribution is being controlled by ciliary beating? What mechanisms determine the direction of ciliary rotation within each ciliated cell? Why is *Nodal* the first asymmetrically expressed gene common to all vertebrates, whereas other factors are variable? And in the chick embryo, the earliest molecular asymmetry seems to be the right-sided localization of the *Activin-receptor IIA*[3] just before the earliest expression of *LRD* and the appearance of nodal cilia[1], which raises the question of whether other symmetry-breaking mechanisms might exist at earlier stages of development. ■

Claudio D. Stern is in the Department of Anatomy and Developmental Biology, University College London, Gower Street, London WC1E 6BT, UK.
e-mail: c.stern@ucl.ac.uk

1. Essner, J. J. *et al. Nature* **418,** 37–38 (2002).
2. Nonaka, S., Shiratori, H., Saijoh, Y. & Hamada, H. *Nature* **418,** 96–99 (2002).
3. Levin, M., Johnson, R. L., Stern, C. D., Kuehn, M. & Tabin, C. *Cell* **82,** 803–814 (1995).
4. Supp, D. M., Witte, D. P., Potter, S. S. & Brueckner, M. *Nature* **389,** 963–966 (1997).
5. Nonaka, S. *et al. Cell* **95,** 829–837 (1998).
6. Okada, Y. *et al. Mol. Cell* **4,** 459–468 (1999).
7. Dunn, G. A. & Ireland, G. W. *Nature* **312,** 63–65 (1984).

Materials science

Crystallization of silicon ideas

John Robertson

The more desirable form of silicon for use in display screens is also the more expensive to manufacture. Understanding how crystalline silicon forms could be a key to cheaper communications devices.

Amorphous silicon is the leading electronic material for large-area applications, used in solar cells and in the thin-film transistors that make up liquid-crystal displays. However, amorphous silicon suffers from an electrical instability that causes a gradual loss of conversion efficiency in solar cells. There is another form of silicon, nanocrystalline silicon, that is more stable and whose charge-carriers (electrons and holes) are more mobile, making it more attractive for use in these applications.

Amorphous silicon can be made easily by deposition from a silane (SiH_4) plasma, and nanocrystalline silicon can be made by the same process, under slightly modified conditions. But the exact means by which nanocrystalline silicon, rather than amorphous silicon, forms has been the subject of debate. Now Sriraman and colleagues[1] might have found the answer: on page 62 of this issue, they propose that hydrogen atoms from the silane plasma catalyse the rearrangement of Si–Si bonds, triggering a solid-state transformation of the random amorphous-silicon network into the more ordered network of nanocrystalline silicon.

Nanocrystalline silicon can be deposited from a silane plasma that has been heavily diluted with hydrogen so that there is a high concentration of atomic hydrogen in the plasma. The most popular explanation of the deposition process has been that nanocrystalline silicon and amorphous silicon are deposited simultaneously, and then the atomic hydrogen etches away amorphous silicon more quickly, leaving mostly nanocrystalline silicon[2]. Once formed, the two solid phases can then only interconvert via the gas phase.

An alternative explanation is that atomic hydrogen permeates the film of amorphous silicon, lowering the energy barriers to the rearrangement of the silicon network into a more stable, more ordered nanocrystalline lattice[3]. But, until now, the precise mecha-

Genome sequencing

Stick it in the family album

You may feel that you have some relations that resemble the cellular slime mould *Dictyostelium discoideum*, shown here. If so, you would be right. For years there has been debate about where this organism sits on the tree of life, and whether it belongs with plants or animals. But a partial genomic sequence — that of chromosome 2, described by Gernot Glöckner *et al.* in this issue (*Nature* **418,** 79–85; 2002) — confirms its closer kinship with animals.

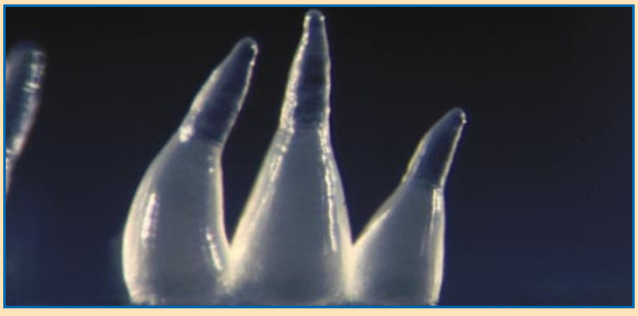

R. KAY/MRC

Dictyostelium — *Dicty* to its friends — is a soil amoeba but nonetheless a eukaryote: an organism with a membrane-bound nucleus. It has long been recognized as an excellent model organism. It shows much of the genetic flexibility of yeast, and has complex signalling pathways as well as chemical-sensing behaviours like those seen, for instance, in white blood cells.

A multinational team of sequencing centres (www.uni-koeln.de/dictyostelium/consortium.shtml) is sequencing the roughly 34 million bases of the *Dicty* genome and mining them for insights into eukaryotic life. But sequencing is dogged by the problem of high A–T base-pair content, and subsequent analysis is also challenging because of the high repetitive content (around 10%).

To surmount some of the hurdles in sequencing, the various groups constructed libraries from each chromosome separately and carried out shotgun sequencing on each library. But the chromosomal libraries are only about 60% pure, so each group is also generating a whole-genome shotgun. By pooling the data from several libraries, Glöckner *et al.* could fish for the maximum number of pieces of chromosome 2 using known chromosome-2 genes as bait. Tying these pieces together and fitting them onto a backbone of clone-based sequences yielded a mostly complete chromosome sequence, which at 8.1 million bases is about 25% of the genome.

Analysis of chromosome 2 indicates that there are 2,799 protein-coding genes and 73 for transfer RNA. On this basis, the entire genome should contain 10,500 to 11,500 genes, with a density similar to that in budding and fission yeasts. Comparison with sequenced eukaryotic genomes revealed about 45% matches to protein-coding genes, and 55% unique to *Dicty*. Although this number seems high, it is in line with estimates for the available sequences of other eukaryotes.

At the same time, analysis of chromosome 2 has already uncovered more family resemblance, as it encodes proteins similar to several cytoskeleton-related and signalling proteins in animals.

With sequences of the remaining five chromosomes coming shortly, *Dicty* will soon need a page in the family photo album. **Chris Gunter**

Conserved function for embryonic nodal cilia

A similar mechanism may underlie the handedness seen in all vertebrate body plans.

How left–right handedness originates in the body plan of the developing vertebrate embryo is a subject of considerable debate[1,2]. In mice, a left–right bias is thought to arise from a directional extracellular flow (nodal flow) that is generated by dynein-dependent rotation of monocilia on the ventral surface of the embryonic node[3,4]. Here we show that the existence of node monocilia and the expression of a dynein gene that is implicated in ciliary function are conserved across a wide range of vertebrate classes, indicating that a similar ciliary mechanism may underlie the establishment of handedness in all vertebrates.

In mice, mutations in the gene that encodes the left–right dynein heavy chain (*Lrd*), a component of the ciliary motor, result in immotile node cilia and a reversal of the left–right (L–R) axis in roughly half of mutant offspring[5,6]. In humans, mutations in the dynein heavy-chain gene *DNAH5* are also associated with immotile cilia syndrome, an inherited disorder that includes mirror-image reversal of the internal organs in half of affected individuals[7]. Both *Lrd* (refs 5, 6) and *Dnahc5* (ref. 7) are expressed in the ventral layer of the mouse node in cells containing cilia (Fig. 1a–c).

To test the validity and universality of the nodal-flow model, we cloned *Lrd* homologues from chick, *Xenopus* and zebrafish, analysed their expression, and examined embryos for the presence of monocilia (see supplementary information). In chick embryos, *Lrdr* (*Lrd*-related) is expressed during gastrulation within Hensen's node and in the primitive streak (Fig. 1d). Although it has been suggested that there is no equivalent of the ventral mouse node in chick[8], we observed cilia at Hensen's node projecting ventrally from the epiblast layer into the space between the dorsal epiblast and the ventral endoderm (Fig. 1e, f).

In *Xenopus*, *Lrdr* is expressed at the end of gastrulation on the ventral side of the dorsal blastopore (Fig. 1g), in cells derived from the early gastrula organizer. At the same time, cilia arise in this region at the completion of gastrulation (Fig. 1h, i). Similarly, a zebrafish *Lrdr* is expressed at the end of gastrulation in the dorsal forerunner cells that migrate ahead of the organizer region (Fig. 1j). Unique to fish, these dorsal forerunner cells give rise during early somite stages to Kupffer's vesicle, a structure that is found in the tail region ventral to the chordal–neural hinge[9]. Strikingly, we found that cells within Kupffer's vesicle also contain monocilia (Fig. 1k, l).

The conservation of nodal cilia and the conserved expression of *Lrd* homologues in different vertebrate model organisms indicate that the activity of nodal cilia is probably a universal mechanism for specifying the vertebrate L–R axis. Previous failures to identify nodal cilia in non-mammals may be related to the differences we have observed in the relative timing and

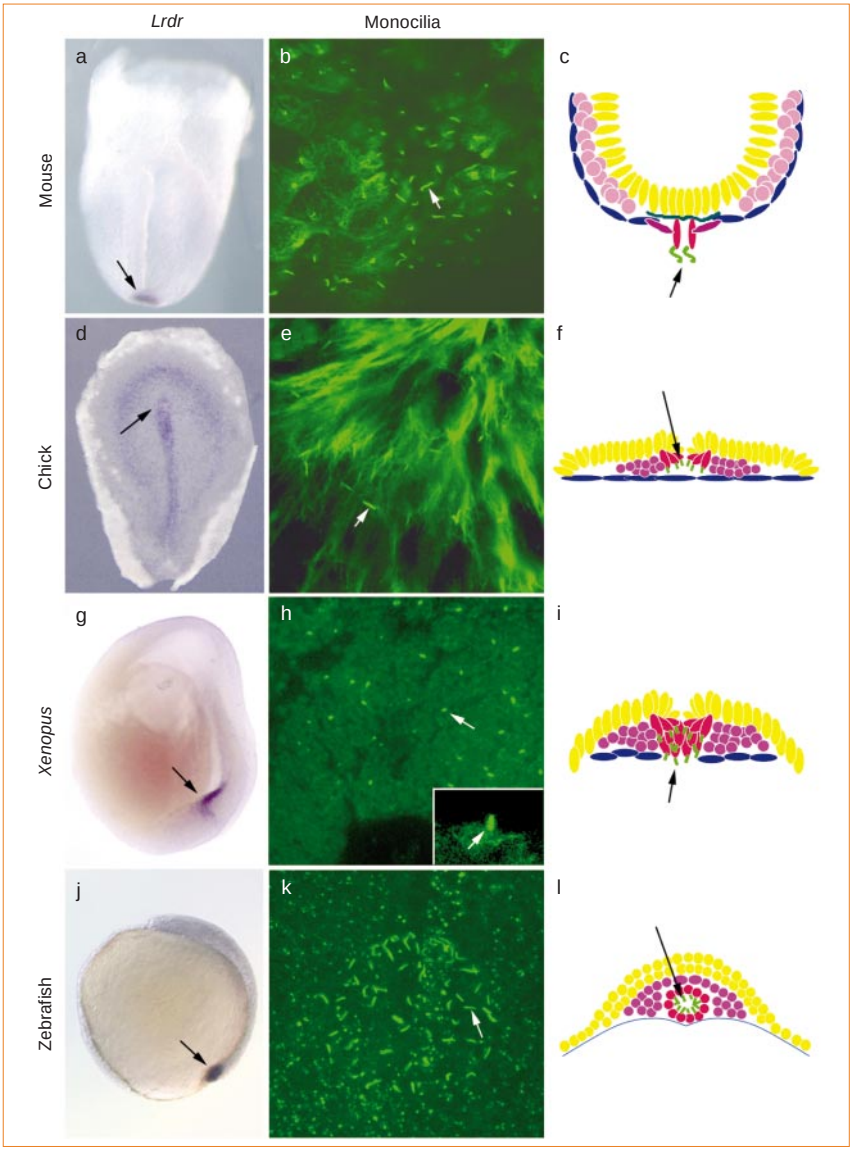

Figure 1 Regions of potential left–right signalling in mouse, chick, *Xenopus* and zebrafish. These regions were identified by *in situ* hybridization with *Lrdr* probes (left) and immunofluorescence with an antibody against acetylated tubulin to detect cilia (centre). Drawings (right) show the locations of ciliated cells. **a,** Frontal view of a mouse embryo 7.5 days post-fertilization (d.p.f.), showing *Lrd* expression at the node. **b,** Ventral view of a mouse embryo at 7.5 d.p.f., showing cilia on the ventral surface of the node. **d,** Dorsal view of a Hamburger–Hamilton (HH) stage 4− chick gastrula-stage embryo showing *Lrdr* expression in Hensen's node and in the primitive streak. **e,** In chick, cilia are present at Hensen's node at HH stage 4− in the space between the dorsal epiblast and the ventral endoderm. **g,** Lateral view of a stage-13 *Xenopus* embryo, showing *Lrdr* expression in the ventral cells of the dorsal blastopore. **h,** After the completion of gastrulation in *Xenopus* (stage 14), cilia begin to form on the ventral surface of the dorsal blastopore. Inset, lateral view of a single cilium. **j,** Lateral view of a late gastrula, or 90% epiboly, zebrafish embryo, showing expression in the dorsal forerunner cells ahead of the organizer region. **k,** In zebrafish at the 10-somite stage (dorsal view), cells in Kupffer's vesicle are ciliated on their inner surface. Anterior is towards the top in all panels; black arrows show regions of *Lrdr* expression where cilia are found (or subsequently develop); white arrows show cilia. **c, f, i, l,** Transverse sections (dorsal is towards the top) showing the locations of ciliated cells (red/green) with respect to the mesoderm (pink), ectoderm (yellow) and endoderm (purple). Arrows indicate the views used in central panels.

Table 1 Nodal cilia features in different vertebrate classes

	Onset of Lrdr mRNA expression	*Appearance of nodal cilia*	*Earliest conserved asymmetric gene expression*
Mouse	Gastrula, 7.5 d.p.f.	Gastrula, 7.5 d.p.f.	*Nodal*, 8.25 d.p.f., 3–5 somites
Chick	Gastrula, HH4 –	Gastrula, HH4 –	*Nodal*, HH7*, 0–2 somites
Xenopus	Stage-11 gastrula	Stage-14 neurula	*Xnr-1* (*Nodal*), stage-17 neurula
Zebrafish	80% epiboly gastrula	Four somites	*Cyclops* (*Nodal*), 20 somites

*Asymmetric gene expression of *Sonic hedgehog* at the node occurs at HH5 (gastrulation) before *Nodal* expression, but seems to be unique to the chick embryo. d.p.f., days post-fertilization.

localization of *Lrdr* expression and formation of nodal cilia. The earliest known asymmetric expression patterns that are common to all vertebrates likewise exhibit considerable variability in their time of onset among different vertebrate classes[1,2]. In all instances, however, these conserved asymmetries are preceded by the onset of *Lrdr* expression and by the appearance of nodal cilia (Table 1), indicating that nodal cilia may be responsible for initiating L–R asymmetric gene expression and for establishing the final body plan in all vertebrates.

Jeffrey J. Essner*, Kyle J. Vogan†, Molly K. Wagner*, Clifford J. Tabin†, H. Joseph Yost*, Martina Brueckner‡

**Center for Children, Huntsman Cancer Institute and Department of Oncological Sciences, University of Utah, Salt Lake City, Utah 84112-5550, USA*
e-mail: joseph.yost@hci.utah.edu
†Department of Genetics, Harvard Medical School, Boston, Massachusetts 02115, USA
‡Department of Pediatrics and Cardiology, Boyer Center for Molecular Medicine, Yale University School of Medicine, New Haven, Connecticut 06520, USA

1. Capdevila, J. *et al. Cell* **101,** 9–21 (2000).
2. Wright, C. V. E. *Dev. Cell* **1,** 179–186 (2001).
3. Nonaka, S. *et al. Cell* **95,** 829–837 (1998).
4. Okada, Y. *et al. Mol. Cell* **4,** 459–468 (1999).
5. Supp, D. M. *et al. Nature* **389,** 963–966 (1997).
6. Supp, D. M. *et al. Development* **126,** 5495–5504 (1999).
7. Olbrich, H. *et al. Nature Genet.* **30,** 143–144 (2002).
8. Männer, J. *Anat. Embryol.* **203,** 481–490 (2001).
9. Cooper, M. S. & D'Amico, L. A. *Dev. Biol.* **180,** 184–198 (1996).

Supplementary information accompanies this communication on *Nature*'s website.
Competing financial interests: declared none.

Gene expression

RNA interference in adult mice

RNA interference is an evolutionarily conserved surveillance mechanism that responds to double-stranded RNA by sequence-specific silencing of homologous genes. Here we show that transgene expression can be suppressed in adult mice by synthetic small interfering RNAs and by small-hairpin RNAs transcribed *in vivo* from DNA templates. We also show the therapeutic potential of this technique by demonstrating effective targeting of a sequence from hepatitis C virus by RNA interference *in vivo*.

Small interfering RNAs (siRNAs) mimic intermediates in the RNA-interference (RNAi) pathway and can silence genes in somatic cells without activating non-specific suppression by double-stranded RNA-dependent protein kinase[1]. To investigate whether siRNAs also inhibit gene expression *in vivo*, we used a modification of hydrodynamic transfection methods[2–4] to deliver naked siRNAs to the livers of adult mice. Either an siRNA derived from firefly luciferase or an unrelated siRNA was co-injected with a luciferase-expression plasmid (for construct description and sequences, see supplementary information). We monitored luciferase expression in living animals using quantitative whole-body imaging[5] (Fig. 1a, c), and found that it was dependent on reporter-plasmid dose (results not shown).

In each experiment, serum measurements of a co-injected human α-1 antitrypsin (hAAT) plasmid[6] served to normalize transfection efficiency and to monitor non-specific translational inhibition. Average serum concentrations of hAAT after 74 h were similar in all groups.

Our results indicate that there was specific, siRNA-mediated inhibition of luciferase expression in adult mice ($P < 0.0115$) and that unrelated siRNAs had no effect ($P < 0.864$; Fig. 1a, b). In 11 independent experiments, luciferase siRNAs reduced luciferase expression (as judged by emitted light) by an average of 81% (±2.2%). These findings indicate that RNAi can downregulate gene expression in adult mice.

As RNAi degrades respiratory syncitial virus RNAs in culture[7], we investigated whether RNAi could be directed against a human pathogenic RNA expressed in a mouse, namely that of hepatitis C virus (HCV). (Infection by HCV, an RNA virus that infects 1 in 40 people worldwide, is the most common reason for liver transplantation in the United States and Europe.) We fused the NS5B region (non-structural protein 5B, viral-polymerase-encoding region) of this virus with luciferase RNA and monitored RNAi by co-transfection *in vivo*. An

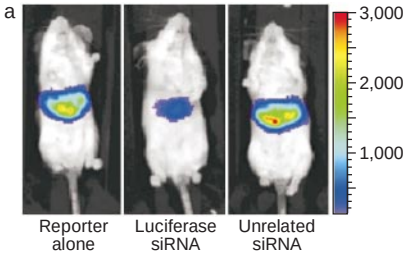

Figure 1 RNA interference in adult mice. **a,** Representative images of light emitted from mice co-transfected with the luciferase plasmid pGL3-control and either no siRNA, luciferase siRNA or unrelated siRNA. A pseudocolour image representing intensity of emitted light (red, most intense; blue, least intense) superimposed on a greyscale reference image (for orientation) shows that RNAi functions in adult mice. Annealed 21-nucleotide siRNAs (40 μg; Dharmacon) were co-injected into the livers of mice with 2 μg pGL3-control DNA (Promega) and 800 units of RNasin (Promega) in 1.8 ml PBS buffer in 5–7 s. After 72 h, mice were anaesthetized and given 3 mg luciferin intraperitoneally 15 min before imaging. **b,** siRNA results (six mice per group) from a representative experiment. Mice receiving luciferase siRNA emitted significantly less light than reporter-alone controls (one-way ANOVA with post hoc Fisher's test). Results for reporter alone and unrelated siRNA were statistically similar. **c,** pShh1-Ff1, but not pShh1-Ff1rev (see text), reduced luciferase expression in mice relative to the reporter-alone control. pShh1-Ff1 or pShh1-rev (10 μg) were co-injected with 2 μg pGL3-control in 1.8 ml PBS buffer. **d,** Average of three independent shRNA experiments ($n = 5$). Average values for the reporter-alone group are designated as 100% in each of the three experiments. Animals were treated according to the US National Institutes of Health's guidelines for animal care and the guidelines of Stanford University.

A

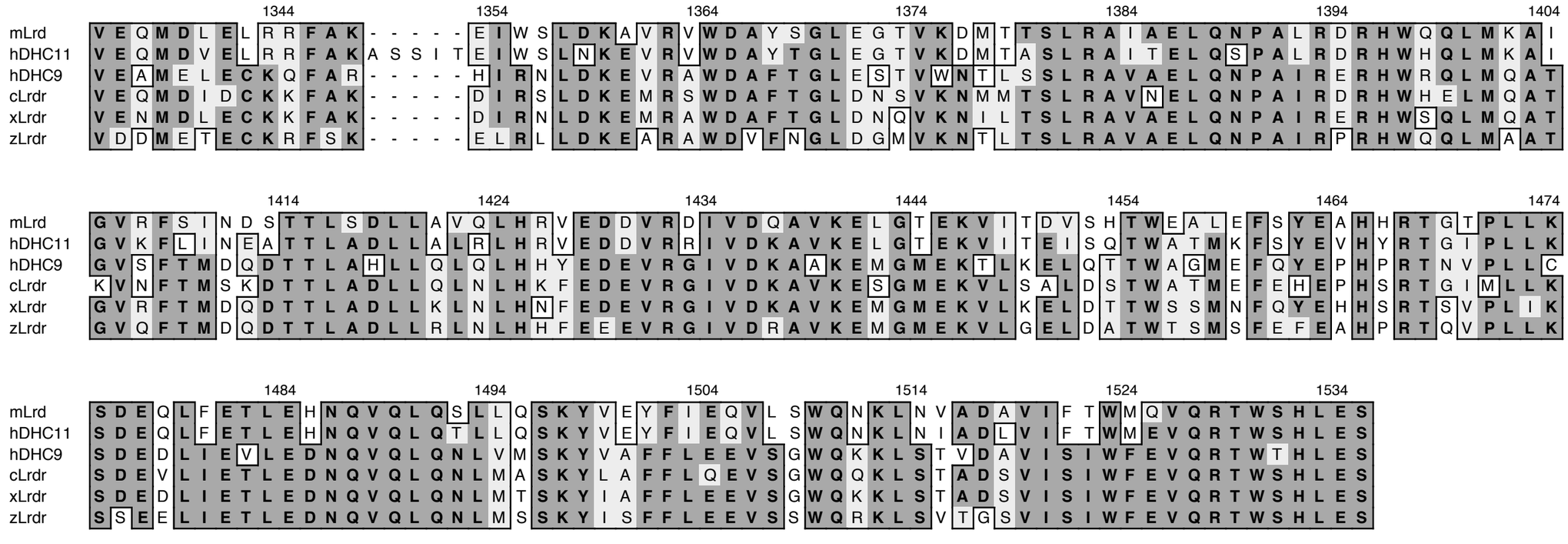

B

	mLRD	hDHC11	hDHC9	cLrdr	xLrdr	zLrdr
mLrd	100%	82%	59%	60%	61%	59%
hDHC11		100%	58%	62%	60%	56%
hDHC9			100%	72%	81%	72%
cLrdr				100%	81%	72%
xLrdr					100%	79%
zLrdr						100%

SUPPLEMENTARY INFORMATION

Based on known axonemal structure, it is predicted that several dynein heavy chains participate in ciliary function during L-R development. For example, both *Lrd* (*Dnahc11*) and *Dnahc5* are expressed in the ventral node in mouse, and mutations in human *DNAH5* are associated with randomization of L-R asymmetry (see main text). In this regard, it is worth noting that the Lrd homologs we isolated from chick (Genbank #AY099489), *Xenopus* (Genbank #AY100020), and zebrafish (Genbank #AY100021) all share a high degree of sequence identity and structural conservation with mouse Lrd (Dnahc11) and human DNAH11 (Fig.2a). However, in the region examined (amino acids 1334-1530 of mouse Lrd), the Lrd homologs we isolated display a higher identity to human DNAH9 than to human DNAH11 (Fig.2b).

Supplementary Figure Legend

a, Alignment showing structural conservation between human, mouse, chick, *Xenopus*, and zebrafish dynein heavy chain sequences. Only the region of overlap for all sequences is shown (amino acids 1334-1529 of mouse Lrd). Dark gray boxes show amino acid identity while light gray boxes represent similarity. Abbreviations are as follows: h, human; m, mouse, c, chick; x, *Xenopus*; z, zebrafish. **b,** Amino acid identity shared between dynein heavy chain proteins.

Methods

Isolation of Lrd homologs by reverse transcription polymerase chain reaction (RT-PCR).

RNA was isolated from gastrula stage chick, *Xenopus*, and zebrafish embryos at Hamburger-Hamilton stage 4, stage 11, and 60% epiboly, respectively, by Trizol extraction (BRL). Reverse transcription of total RNA was performed with Superscript (BRL) using a degenerate primer (5'-CAR TTR AAN ACR TAN ACC AT-3'), and PCR amplifications were carried out using Platinum Taq (BRL). From chick, three overlapping fragments corresponding to amino acids 1334-2209 of mouse Lrd were amplified as follows. First, a 800 bp fragment corresponding to amino acids 1334-1600 of mouse Lrd was amplified using the following primers: 5'-CAR TTY AAR GAR CAR ATH GA-3' and 5'-TCT CCA GGT ACT CGG CCA RNG CYT TYT C-3'. Second, a 523 bp fragment corresponding to amino acids 2036-2209 of mouse Lrd was amplified using the following primers: 5'-GAG CTG CTG TCC AAR CAG GAT G-3' and 5'-AAG AGA CCA TCT TTC CAT TCT T-3'. Finally, the intervening 1.4 Kb sequence was amplified using the following specific primers: 5'-CTG GAG GCA CTG CAG AAG AG-3' and 5'-CCA GCA CTG ACT TGA TAC CAC-3'. From *Xenopus*, a 1.5 Kb fragment corresponding

to amino acids 1061-1605 of mouse Lrd was amplified using the following degenerate primers: 5'-CAR TTY AAR GAR CAR ATH GA-3' and 5-TGN ARY TGN ACY TGR TTR TG-3'. From zebrafish a 600 bp fragment corresponding to amino acids 1334-1530 of mouse Lrd was amplified using the following primers: 5'-CCC AGT GGC GGG AGA THA AYG TNG A-3' and 5-GGA CTC CAG GTG GGA CCA NGT NCK YTG-3. All amplified fragments were cloned into pCRII using the Topo cloning kit (Invitrogen) and subsequently sequenced.

***In situ* hybridization and immunofluorescence**

In situ hybridizations were performed according to standard protocols. For immunofluoresence studies, mouse and chick embryos were fixed for 2 hours at room temperature in 4% paraformaldehyde in PEMT (80 mM PIPES pH 7.4, 500 nM Taxol, 1mM EGTA, 1mM $MgCl_2$, 0.2% TritonX-100). *Xenopus* and zebrafish embryos were fixed in 4% paraformaldehyde in PBS at room temperature for one hour followed by overnight at 4 ^{o}C. Immunofluorescence was performed according to standard protocols using a mouse anti-acetylated tubulin monoclonal antibody (Sigma) at a 1:150 dilution (for mouse and chick embryos) or at a 1:400 dilution (for *Xenopus* and zebrafish embryos). For secondary antobodies, either Alexa 488-conjugated goat anti-mouse antibodies (Molecular Probes) were used at a 1:200 dilution (for mouse and chick embryos) or FITC-conjugated goat anti-mouse IgG2b antibodies (Southern Biotechnology Associates, Inc) were used at a 1:500 dilution (for Xenopus and zebrafish embryos). Mouse and chicken embryos were mounted in Pro-Long antifade (Molecular Probes), while *Xenopus* and zebrafish embryos were placed in Slow Fade (Molecular Probes). *Xenopus* and zebrafish embryos were imaged on an Olympus Fluoview Scanning Laser microscope using a 60X objective.

they responded to forskolin stimulation, and cAMP transients were scored only if 520- and 580-nm traces changed in opposite directions. Statistical analysis was performed using the Kolmogorov–Smirnov non-parametric test; values are presented as mean ± s.e.m. and were considered significantly different for $P < 0.05$.

Computation

Constants in the model are annotated in Supplementary Information; MATLAB 6.0 (Mathworks) was used for numerical calculations. Wavelet analysis was performed using the Morlet wavelet from the standard numerical 'wavelet analysis' package (Mathworks). Wavelet analysis produces a set of coefficients, C_{ab}, calculated using the formula $C_{ab} \approx \int \mathrm{d}t f(t) \Psi[(t-a)/b]$, where Ψ is the analysing function referred to as the 'wavelet', a represents time localization and b is the scale, which is inversely proportional to the local frequency. To avoid edge effects, only the central 40 min of each hour were considered. No periodic structure was evident when this method was tested with white noise.

Received 28 December 2001; accepted 22 April 2002; doi:10.1038/nature00835.

1. Cuthbertson, K. S. & Cobbold, P. H. Phorbol ester and sperm activate mouse oocytes by inducing sustained oscillations in cell Ca^{2+}. *Nature* **316,** 541–542 (1985).
2. Kline, D. & Kline, J. T. Repetitive calcium transients and the role of calcium in exocytosis and cell cycle activation in the mouse egg. *Dev. Biol.* **149,** 80–89 (1992).
3. Gu, X. & Spitzer, N. C. Distinct aspects of neuronal differentiation encoded by frequency of spontaneous Ca^{2+} transients. *Nature* **375,** 784–787 (1995).
4. Fields, R. D., Eshete, F., Stevens, B. & Itoh, K. Action potential-dependent regulation of gene expression: temporal specificity in Ca^{2+}-cAMP-responsive element binding proteins, and mitogen-activated protein kinase signalling. *J. Neurosci.* **17,** 7252–7266 (1997).
5. Carey, M. B. & Matsumoto, S. G. Spontaneous calcium transients are required for neuronal differentiation of murine neural crest. *Dev. Biol.* **215,** 298–313 (1999).
6. Wayman, G. A., Hinds, T. R. & Storm, D. R. Hormone stimulation of type III adenylyl cyclase induces Ca^{2+} oscillations in HEK-293 cells. *J. Biol. Chem.* **270,** 24108–24115 (1995).
7. Rasmussen, H. *Calcium and cAMP as Synarchic Messengers* (Wiley, New York, 1981).
8. Ming, G. L. *et al.* cAMP-dependent growth cone guidance by netrin-1. *Neuron* **19,** 1225–1235 (1997).
9. Mons, N., Decorte, L., Jaffard, R. & Cooper, D. M. F. Ca^{2+}-sensitive adenylyl cyclases, key integrators of cellular signalling. *Life Sci.* **62,** 1647–1652 (1998).
10. Bhalla, U. S. & Iyengar, R. Emergent properties of networks of biological signalling pathways. *Science* **283,** 381–387 (1999).
11. Hartwell, L. H., Hopfield, J. J., Leibler, S. & Murray, A. W. From molecular to modular cell biology. *Nature* **402 suppl.,** C47–C52 (1999).
12. Tang, Y. & Othmer, H. G. Frequency encoding in excitable systems with applications to calcium oscillations. *Proc. Natl Acad. Sci. USA* **92,** 7869–7873 (1995).
13. Islam, M. S. *et al. In situ* activation of the type 2 ryanodine receptor in pancreatic beta cells requires cAMP-dependent phosphorylation. *Proc. Natl Acad. Sci. USA* **95,** 6145–6150 (1998).
14. Haug, L. S., Jensen, V., Hvalby, O., Walaas, S. I. & Ostvold, A. C. Phosphorylation of the inositol 1,4,5-trisphosphate receptor by cyclic nucleotide-dependent kinases *in vitro* and in rat cerebellar slices *in situ*. *J. Biol. Chem.* **274,** 7467–7473 (1999).
15. Eliot, L. S., Dudai, Y., Kandel, E. R. & Abrams, T. W. Ca^{2+}/calmodulin sensitivity may be common to all forms of neural adenylate cyclase. *Proc. Natl Acad. Sci. USA* **86,** 9564–9568 (1989).
16. Sette, C., Vicini, E. & Conti, M. The rat PDE3/IVd phosphodiesterase gene codes for multiple proteins differentially activated by cAMP-dependent protein kinase. *J. Biol. Chem.* **269,** 18271–18274 (1994).
17. Beck, F., Blasius, B., Luttge, U., Neff, R. & Rascher, U. Stochastic noise interferes coherently with a model biological clock and produces specific dynamic behaviour. *Proc. R. Soc. Lond. B* **268,** 1307–1313 (2001).
18. Woods, N. M., Cuthbertson, K. S. & Cobbold, P. H. Repetitive transient rises in cytoplasmic free calcium in hormone-stimulated hepatocytes. *Nature* **319,** 600–602 (1986).
19. Berridge, M. J. & Galione, A. Cytosolic calcium oscillators. *FASEB J.* **2,** 3074–3082 (1988).
20. Fewtrell, C. Ca^{2+} oscillations in non-excitable cells. *Annu. Rev. Physiol.* **55,** 427–454 (1993).
21. Goldbeter, A., Dupont, G. & Halloy, J. The frequency encoding of pulsatility. *Novartis Found. Symp.* **227,** 19–36 (2000).
22. Haisenleder, D. J., Yasin, M. & Marshall, J. C. Gonadotropin subunit and gonadotropin-releasing hormone receptor gene expression are regulated by alterations in the frequency of calcium pulsatile signals. *Endocrinology* **138,** 5227–5230 (1997).
23. Villalobos, C., Faught, W. J. & Frawley, L. S. Dynamic changes in spontaneous intracellular free calcium oscillations and their relationship to prolactin gene expression in single, primary mammotropes. *Mol. Endocrinol.* **12,** 87–95 (1998).
24. Dolmetsch, R. E., Xu, K. L. & Lewis, R. S. Calcium oscillations increase the efficiency and specificity of gene expression. *Nature* **392,** 933–936 (1998).
25. Kaang, B. K., Kandel, E. R. & Grant, S. G. Activation of cAMP-responsive genes by stimuli that produce long-term facilitation in *Aplysia* sensory neurons. *Neuron* **10,** 427–435 (1993).
26. Haisenleder, D. J., Yasin, M. & Marshall, J. C. Enhanced effectiveness of pulsatile 3′5′ cyclic adenosine monophosphate in stimulating prolactin and alpha-subunit expression. *Endocrinology* **131,** 3027–3033 (1992).
27. Bacskai, B. J. *et al.* Spatially resolved dynamics of cAMP and protein kinase A subunits in *Aplysia* sensory neurons. *Science* **260,** 222–226 (1993).
28. Montarolo, P. G. *et al.* A critical period for macromolecular synthesis in long-term heterosynaptic facilitation in *Aplysia*. *Science* **234,** 1249–1254 (1986).
29. Cooper, D. M. F., Mons, N. & Karpen, J. W. Adenylyl cyclases and the interaction between calcium and cAMP signalling. *Nature* **374,** 421–424 (1995).
30. Berridge, M. J., Lipp, P. & Bootman, M. D. The versatility and universality of calcium signalling. *Nature Rev. Mol. Cell. Biol.* **1,** 11–21 (2000).

Supplementary Information accompanies the paper on *Nature*'s website (http://www.nature.com/nature).

Acknowledgements

We thank S. R. Adams, T. M. Gomez, I. Hsieh and N. Lautermilch for assistance, A. Rozhkov for advice on modeling, and P. H. Diamond, M. B. Feller and T. M. Gomez for comments on the manuscript. This work was supported by a Burroughs-Wellcome LJIS fellowship (Y.V.G.) and NIH NINDS grant (N.C.S.).

Competing interests statement

The authors declare that they have no competing financial interests.

Correspondence and requests for materials should be addressed to N.C.S. (e-mail: nspitzer@ucsd.edu).

Determination of left–right patterning of the mouse embryo by artificial nodal flow

Shigenori Nonaka, Hidetaka Shiratori, Yukio Saijoh & Hiroshi Hamada

Graduate School of Frontier Biosciences, Osaka University, 1–3 Yamada-oka, Suita, Osaka 565-0871, Japan; and CREST, Japan Science and Technology Corporation (JST), Japan

Substantial insight has recently been achieved into the mechanisms responsible for the generation of left–right (L–R) asymmetry in the vertebrate body plan[1–4]. However, the mechanism that underlies the initial breaking of symmetry has remained unclear. In the mouse, a leftward fluid flow on the ventral side of the node caused by the vortical motion of cilia (referred to as nodal flow) is implicated in symmetry breaking[5], but direct evidence for the role of this flow has been lacking. Here we describe the development of a system in which mouse embryos are cultured under an artificial fluid flow and with which we have examined how flow affects L–R patterning. An artificial rightward flow that was sufficiently rapid to reverse the intrinsic leftward nodal flow resulted in reversal of situs in wild-type embryos. The artificial flow was also able to direct the situs of mutant mouse embryos with immotile cilia. These results provide the first direct evidence for the role of mechanical fluid flow in L–R patterning.

The breaking of symmetry during vertebrate development is thought to occur in or near the node. In the mouse embryo, the ventral surface of the node (nodal pit) possesses several hundred monocilia[6] that rotate in a clockwise direction, and this rotational movement somehow generates a leftward laminar flow[5]. The lack of this nodal flow as a result of impaired ciliary development leads to randomization of body situs[5,7–10]. Nodal flow has thus been proposed to trigger a signalling cascade responsible for L–R patterning by transporting an unidentified molecule towards the left side of the body. However, this 'nodal flow hypothesis' has remained unproved. It raises many questions, the most important of which is whether the nodal flow is a genuine symmetry-breaking event or simply a manifestation of such an event.

One approach to test directly the role of nodal flow would be to manipulate the flow mechanically and to examine how such manipulation affects L–R patterning. To achieve this goal, we developed a culture system (flow culture) in which embryos are allowed to develop under a constant flow of culture medium driven by a peristaltic pump (Fig. 1a). In this system, octopus-trap-like pots hold embryos in their proximal region (Fig. 1b, c), so that the distal region, including the node, is exposed to the flow. The artificial flow can be controlled in two ways: First, the flow can be leftward (Fig. 1b) or rightward (Fig. 1c) with respect to the L–R axis of the embryo, depending on how the embryos are placed in the pots. Second, the rate of the flow can be adjusted to either fast or slow.

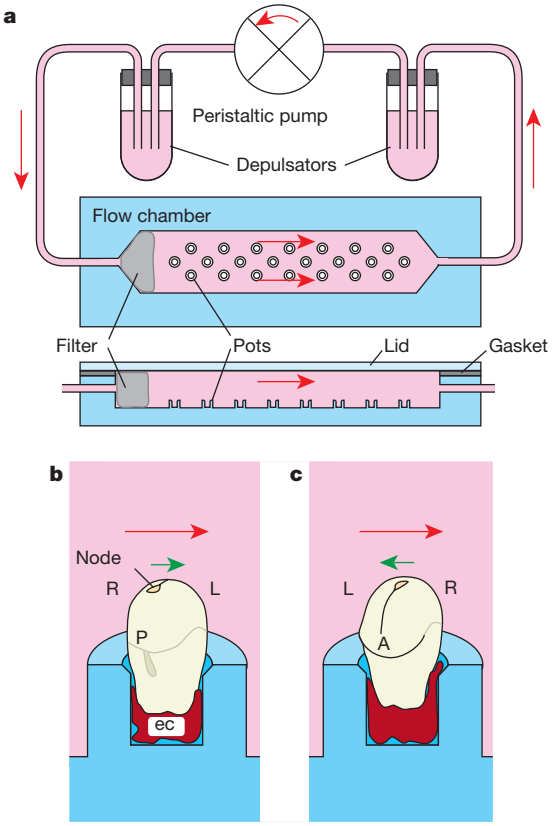

Figure 1 Flow culture system. **a**, Schematic representation of the flow culture system. The peristaltic pump and depulsators ensure constant circulation of culture medium. The filter located at the entrance of the flow chamber prevents turbulence in the chamber. **b**, **c**, Relation between the direction of the intrinsic nodal flow (green arrow) and that of the pump-driven artificial flow (red arrow). Artificial flow is leftward in **b** and rightward in **c**, with respect to the L–R axis of each embryo. The ectoplacental cone (ec) serves as a glue to stabilize the position of the embryo. A, P, L and R refer to the anterior, posterior, left and right sides of the embryo, respectively.

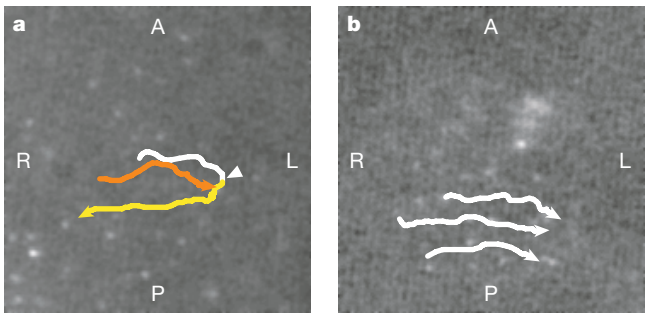

Figure 2 Reversal of the intrinsic nodal flow by fast, but not by slow, rightward artificial flow. Embryos at the one-somite stage were placed in the flow chamber as depicted in Fig. 1c, and the fluid flow in the node was visualized with fluorescent beads. Arrows indicate the direction of individual beads. Video clips of bead motion are provided in the Supplementary Information. **a**, Fast rightward flow. The pump was initially off, then it was turned on to impose the fast rightward flow, and it was then turned off again. In the absence of the artificial flow, a bead moved leftward (white line), but it turned rightward (yellow line) when the pump started (arrowhead). After the pump stopped, a bead resumed its original leftward movement (orange line). The bead travelled along the L–R axis at the speed of 12.9 $\mu m\,s^{-1}$ (white line), 14.5 $\mu m\,s^{-1}$ (yellow line), and 16.3 $\mu m\,s^{-1}$ (orange line). **b**, Slow rightward flow. The flow in the node was observed under the slow rightward flow. The flow remained leftward even when the slow rightward flow was imposed (white lines). Three beads from the top travelled along the L–R axis at the speed of 19.4 $\mu m\,s^{-1}$, 16.1 $\mu m\,s^{-1}$ and 22.4 $\mu m\,s^{-1}$, respectively. A, P, L and R refer to anterior, posterior, left and right sides of the node, respectively.

According to hydrodynamics, the rate of fluid flow decreases in the region near the surface of an object. This principle results in the formation of a velocity gradient of the pump-driven flow in the vicinity of each embryo, with the flow rate decreasing as the distance to the embryo shortens. Given that nodal flow occurs only within a distance of several micrometres from the surface of the node, the pump-driven flow in this region would be expected to exert limited influence compared with that predicted from the average flow rate in the chamber. It was therefore essential to examine how endogenous nodal flow was affected by the pump-driven flow. Although we tested several different speeds, we describe the effects of two rates of pump-driven flow in the following experiments: fast flow (average speed in the chamber of 110 $\mu m\,s^{-1}$) and slow flow (average speed in the chamber of 5.7 $\mu m\,s^{-1}$). Mouse embryos were cultured under conditions of fast flow or slow flow, and the fluid flow within the node was visualized with fluorescent beads. Fast rightward flow in the chamber was sufficient to reverse the intrinsic nodal flow of the normal mouse embryo (Fig. 2a; Supplementary Information 1), whereas slow rightward flow was not (Fig. 2b; Supplementary Information 2). Leftward flow in the chamber, either fast or slow, did not change the direction of the fluid flow in the node (data not shown).

We next tested four types of artificial flow (leftward or rightward, fast or slow) for their effects on L–R patterning. Mouse embryos at the presomite stage were cultured in the flow chamber for 14 h, followed by conventional rotation culture[11] for an additional 32 h. At the end of the incubation, the directions of heart looping and embryonic turning were examined. The *Pitx2-lacZ* transgene (*17-P1*)[12] was also used as a marker for L–R patterning, and embryos harbouring this construct were stained with the β-galactosidase substrate X-gal. Under conditions of fast leftward or slow leftward flow, most wild-type embryos developed a normal L–R axis (Fig. 3a, b, h). They thus manifested dextral heart looping (D-looping) and normal embryonic turning. The *Pitx2-lacZ* transgene exhibited normal left-sided expression in the common atrium chamber, and left-sided or bilateral expression in the truncus arteriosus. When the embryos treated with fast leftward flow were recovered earlier (after 10 h of rotation culture instead of 32 h), *Pitx2-lacZ* showed left-sided expression in the lateral plate (Fig. 3i). In contrast, fast rightward flow efficiently reversed the L–R markers of wild-type embryos (Fig. 3d, j, k, l). Thus, most of the embryos exhibited reversed heart looping (L-looping), reversed turning, and right-sided expression of *Pitx2-lacZ* and *nodal*. Slow rightward flow, which was not fast enough to reverse the direction of the endogenous nodal flow (Fig. 2b), failed to induce frequent reversal of L–R situs (Fig. 3c). The effects of fast rightward flow were dependent on embryo stage. Whereas embryos at the presomite stage were sensitive to fast rightward flow, those at the one-somite (Fig. 3e), two-somite (Fig. 3f), or three-somite (Fig. 3g) stage were not.

We performed similar experiments with homozygous *inversus viscerum* (*iv*/*iv*) mutant embryos, which both lack nodal flow because the monocilia in the node are immotile[7,9] and exhibit randomized L–R patterning (half of *iv*/*iv* homozygotes thus develop situs inversus). If the lack of nodal flow is responsible for the observed L–R defects in *iv*/*iv* embryos, then an artificial flow that mimics the nodal flow might be expected to rescue the phenotype. Indeed, *iv*/*iv* embryos cultured at the presomite stage under conditions of fast leftward or slow leftward flow manifested normal turning, D-looping of the heart tube, and left-sided expression of the *Pitx2-lacZ* transgene (Fig. 4a, b). In contrast, most *iv*/*iv* embryos subjected to fast rightward or slow rightward flow exhibited reversal of L–R situs (Fig. 4c, d). Although slow rightward flow was unable to change the direction of the endogenous nodal flow of wild-type embryos (Fig. 2b), slow flow was able to induce L–R patterning in *iv*/*iv* embryos with immotile cilia.

The changes in L–R patterning induced by artificial fluid flow are unlikely to be due to nonspecific effects of the *in vitro* culture. First, embryos subjected to rightward and leftward flows were cultured

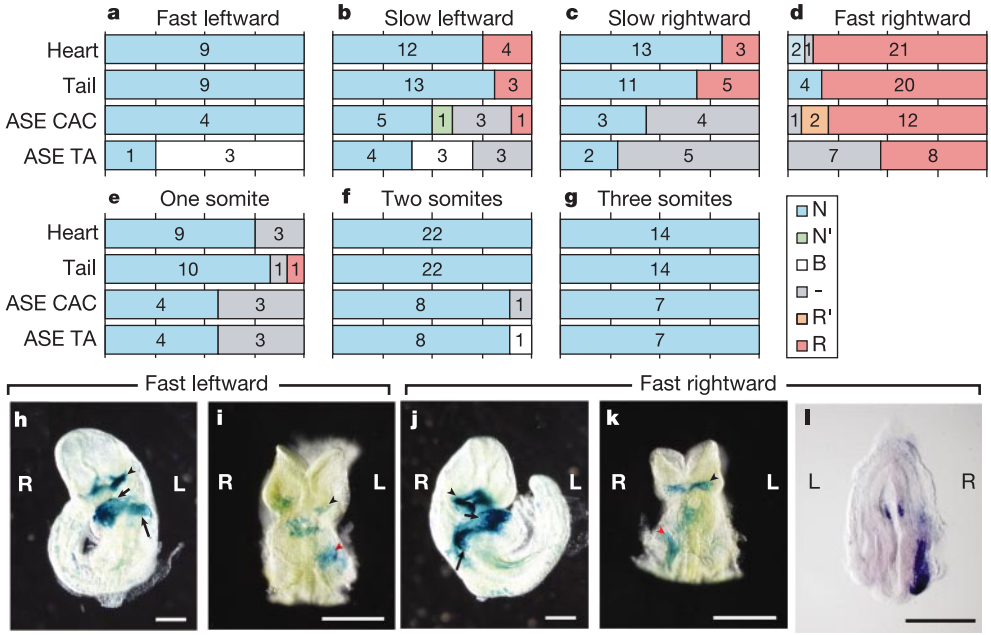

Figure 3 Reversal of situs of wild-type embryos at the presomite stage by fast rightward flow. The effects of artificial fluid flow on various L–R markers were evaluated. **a**–**d**, Mouse embryos at the presomite stage were cultured under the indicated conditions of artificial flow. Most embryos subjected to fast (**a**) or slow (**b**) leftward flow or to slow rightward flow (**c**) developed normal situs. In contrast, fast rightward flow (**d**) resulted in reversal of situs in most embryos. **e**–**g**, Embryos at the one-somite (**e**), two-somite (**f**), or three-somite (**g**) stage were insensitive to fast rightward flow. Colour scale: N, normal patterns (D-looping for the heart, right-sided tail for embryonic turning, and left-sided expression for *Pitx2-lacZ*); N′, bilateral expression of *Pitx2-lacZ*, with a higher level of expression on the left side; B, bilaterally equal expression of *Pitx2-lacZ*; (−), absence of L–R markers (outloop in the heart, no embryonic turning, and no *Pitx2-lacZ* expression); R′, bilateral expression of *Pitx2-lacZ*, with a higher level of expression on the right side; R, inverted patterns (L-looping for the heart, left-sided tail for embryonic turning, and right-sided expression for *Pitx2-lacZ*). CAC, common atrium chamber; TA, truncus arteriosus; ASE, transgene expression determined by the asymmetric enhancer of *Pitx2*. Numbers refer to the number of embryos with the indicated properties among the total examined. **h**, Presomite-stage embryo subjected to fast leftward flow and then stained with X-gal. D-looping of the heart, normal turning, left-sided X-gal staining in the CAC (long arrow), and bilateral X-gal staining in the TA (short arrow) are apparent. Bilateral staining in the first branchial arch (arrowhead) is also characteristic of this transgene[12]. **i**, Presomite-embryo treated with fast leftward flow was recovered earlier (after 10 h of rotation culture instead of the typical 32 h) and was stained with X-gal. Left-sided staining in the lateral plate (red arrowhead) and bilateral staining in the branchial arch (black arrowhead) are apparent. **j**, Presomite-stage embryo subjected to fast rightward flow and then stained with X-gal. L-looping of the heart, reversed turning, right-sided X-gal staining in the CAC (long arrow) and TA (short arrow) are apparent. The first branchial arch is indicated with a black arrowhead. **k**, Presomite-embryo treated with fast rightward flow was recovered earlier (after 10 h of rotation culture instead of the typical 32 h) and was stained with X-gal. Right-sided staining is apparent in the lateral plate (red arrowhead). The first branchial arch is indicated with a black arrowhead. **l**, Presomite-embryos treated with fast rightward flow were recovered earlier and were examined for *nodal* expression by *in situ* hybridization. *nodal* expression in the lateral plate was right-sided. All scale bars, 0.5 mm.

simultaneously in the same chamber (Fig. 1b, c), but the effects on L–R patterning were specific to the direction of the artificial flow with respect to the L–R axis of each embryo. Second, whereas the slow rightward flow failed to affect the situs of wild-type embryos, it induced reversal of situs in *iv*/*iv* embryos. Furthermore, whereas embryos at the presomite stage were sensitive to the fast rightward flow, those at slightly later stages of development were not, suggesting that L–R determination is still undetermined at the presomite stage. This notion is consistent both with the previous observation that nodal flow begins at the presomite stage (the late neural-fold stage)[7], before asymmetric expression of *nodal* and *lefty* has begun[13–16], as well as with the previous suggestion that the L–R axis of the rat embryo is determined at the equivalent stage[17].

Our results provide the first direct evidence for the role of mechanical fluid flow in L–R determination. In the flow culture system, the surface of the whole embryos was subjected to the current of media. However, it is most probably the alteration of flow in the node that resulted in situs reversal because the node is the only region of the embryo surface where the intrinsic directional flow has been detected. Of the questions that remain unanswered, one of the most important concerns the mechanism by which the vectorial flow is generated by the rotational movement of the cilia. Hydrodynamic considerations may provide some insight: it will be essential to characterize precisely the movement and morphology of the cilia, the shape of the node and the hydrodynamic properties of the nodal flow. □

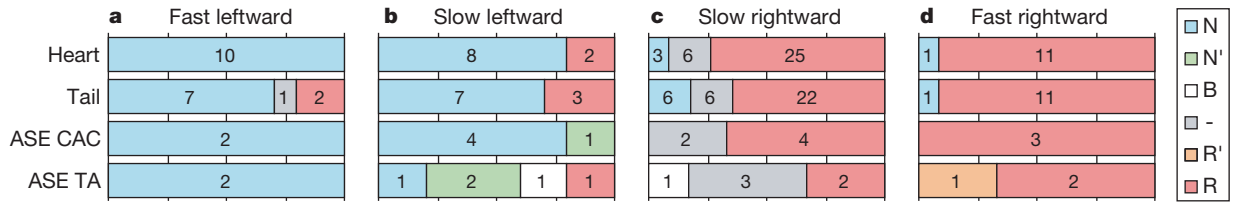

Figure 4 Determination of situs of *iv*/*iv* embryos by artificial fluid flow. Presomite-stage *iv*/*iv* embryos were incubated under the indicated conditions of artificial flow, the effects of which were then evaluated as described in Fig. 3. Fast (**a**) and slow (**b**) leftward flows mostly gave rise to normal situs, whereas slow (**c**) and fast (**d**) rightward flows induced reversal of situs. Colour scale as in Fig. 3.

Methods

Flow culture

Male mice harbouring a *Pitx2-lacZ* transgene (*17-P1*, a transgene that recapitulates the asymmetric expression of *Pitx2*)[12] were crossed with ICR female mice (Charles River). The resulting embryos were dissected at embryonic day 7.7 in Dulbecco's modified Eagle's medium (DMEM) supplemented with 10% fetal bovine serum and 25 mM HEPES-NaOH (pH 7.2). Embryos were staged on the basis of their morphology[18], and those between the late-bud and the late-headfold stages were used for flow culture. They were allowed to develop in the flow chamber for 14 h (embryos develop to the four- to seven-somite stage during flow culture; underdeveloped embryos with fewer than four somites were occasionally observed and were discarded without analysis) and were then subjected to conventional rotation culture[11] for an additional 32 h. During this treatment, embryos develop to the stage equivalent to embryonic day 9.5. They were then fixed and stained with X-gal by the standard protocol[11]. The presence of the transgene was determined by X-gal staining at the first branchial arch and by polymerase chain reaction (PCR)-based genotyping. Throughout culture, embryos were maintained at 37 °C under 5% CO_2 and 20% O_2 in standard embryo culture medium composed of 50% rat serum, 50% DMEM buffered with 44 mM $NaHCO_3$ (pH 7.2), penicillin (50 U ml^{-1}), and streptomycin (50 mg ml^{-1}).

Visualization of fluid flow in the node

To visualize fluid flow in the node, we added a 2% solution of 1-μm-diameter red fluorescent polystyrene beads (FluoSphere F-8821, Molecular Probes) at a volume proportion of 1/500 to the culture medium (50% rat serum, 50% DMEM buffered with 25 mM HEPES-NaOH (pH 7.2)). The fluid flow was visualized with the fluorescent beads that were present at a level of approximately 5 μm higher than the surface of the node where the natural nodal flow is most apparent. Fluorescent images were obtained with a monochrome CCD (charge-coupled device) camera (HAS-2000EX, DITECT) connected to a personal computer, and they were processed with Scion Image software.

Received 11 March; accepted 24 April 2002; doi:10.1038/nature00849.

1. Beddington, R. S. & Robertson, E. J. Axis development and early asymmetry in mammals. *Cell* **96,** 195–209 (1999).
2. Capdevila, J., Vogan, K. J., Tabin, C. J. & Izpisua Belmonte, J. C. Mechanisms of left-right determination in vertebrates. *Cell* **101,** 9–21 (2000).
3. Wright, C. V. Mechanisms of left-right asymmetry: What's right and what's left? *Dev. Cell* **1,** 179–186 (2001).
4. Hamada, H., Meno, C., Watanabe, D. & Saijoh, Y. Establishment of vertebrate left-right asymmetry. *Nature Rev. Genet.* **3,** 103–113 (2002).
5. Nonaka, S. *et al.* Randomization of left-right asymmetry due to loss of nodal cilia generating leftward flow of extraembryonic fluid in mice lacking KIF3B motor protein. *Cell* **95,** 829–837 (1998).
6. Sulik, K. *et al.* Morphogenesis of the murine node and notochordal plate. *Dev. Dyn.* **201,** 260–278 (1994).
7. Okada, Y. *et al.* Abnormal nodal flow precedes situs inversus in *iv* and *inv* mice. *Mol. Cell* **4,** 459–468 (1999).
8. Takeda, S. *et al.* Left-right asymmetry and kinesin superfamily protein KIF3A: new insights in determination of laterality and mesoderm induction by *kif3A*$^{-/-}$ mice analysis. *J. Cell Biol.* **145,** 825–836 (1999).
9. Supp, D. M. *et al.* Targeted deletion of the ATP binding domain of left-right dynein confirms its role in specifying development of left-right asymmetries. *Development* **126,** 5495–5504 (1999).
10. Pazour, G. J. *et al.* Chlamydomonas IFT88 and its mouse homologue, polycystic kidney disease gene tg737, are required for assembly of cilia and flagella. *J. Cell Biol.* **151,** 709–718 (2000).
11. Hogan, B. L. *et al. Manipulating The Mouse Embryo: A Laboratory Manual* (Cold Spring Harbor Laboratory Press, Cold Spring Harbor, New York, 1994).
12. Shiratori, H. *et al.* Two-step regulation of left-right asymmetric expression of Pitx2: Initiation by Nodal signalling and maintenance by Nkx2. *Mol. Cell* **7,** 137–149 (2001).
13. Collignon, J., Varlet, I. & Robertson, E. J. Relationship between asymmetric nodal expression and the direction of embryonic turning. *Nature* **381,** 155–158 (1996).
14. Lowe, L. A. *et al.* Conserved left-right asymmetry of nodal expression and alterations in murine situs inversus. *Nature* **381,** 158–161 (1996).
15. Meno, C. *et al.* Left-right asymmetric expression of the TGFβ-family member lefty in mouse embryos. *Nature* **381,** 151–155 (1996).
16. Meno, C. *et al.* Two closely-related left-right asymmetrically expressed genes, *lefty-1* and *lefty-2*: their distinct expression domains, chromosomal linkage and direct neuralizing activity in Xenopus embryos. *Genes Cells* **2,** 513–524 (1997).
17. Fujinaga, M. & Baden, J. M. Critical period of rat development when sidedness of asymmetric body structures is determined. *Teratology* **44,** 453–462 (1991).
18. Downs, K. M. & Davies, T. Staging of gastrulating mouse embryos by morphological landmarks in the dissecting microscope. *Development* **118,** 1255–1266 (1993).

Supplementary Information accompanies the paper on *Nature*'s website (http://www.nature.com/nature).

Acknowledgements

We thank I. Minoura for helpful discussion of hydrodynamics and K. Mochida and other members of the Hamada laboratory for technical help and valuable comments. This work was supported by CREST (Core Research for Evolutional Science and Technology) of the Japan Science and Technology Corporation. S.N. was supported by CREST and by a fellowship from the Japan Society for the Promotion of Science for Japanese Junior Scientists.

Competing interests statement

The authors declare that they have no competing financial interests.

Correspondence and requests for materials should be addressed to S.N. (e-mail: snonaka@fbs.osaka-u.ac.jp) or H.H. (e-mail: hamada@fbs.osaka-u.ac.jp).

AID mutates *E. coli* suggesting a DNA deamination mechanism for antibody diversification

Svend K. Petersen-Mahrt*, Reuben S. Harris* & Michael S. Neuberger

Medical Research Council Laboratory of Molecular Biology, Hills Road, Cambridge CB2 2QH, UK
** These authors contributed equally to this work*

After gene rearrangement, immunoglobulin variable genes are diversified by somatic hypermutation or gene conversion, whereas the constant region is altered by class-switch recombination. All three processes depend on activation-induced cytidine deaminase (AID)[1–7], a B-cell-specific protein that has been proposed (because of sequence homology[1]) to function by RNA editing. But indications that the three gene diversification processes might be initiated by a common type of DNA lesion[8–11], together with the proposal that there is a first phase of hypermutation that targets dC/dG[12], suggested to us that AID may function directly at dC/dG pairs. Here we show that expression of AID in *Escherichia coli* gives a mutator phenotype that yields nucleotide transitions at dC/dG in a context-dependent manner. Mutation triggered by AID is enhanced by a deficiency of uracil-DNA glycosylase, which indicates that AID functions by deaminating dC residues in DNA. We propose that diversification of functional immunoglobulin genes is triggered by AID-mediated deamination of dC residues in the immunoglobulin locus with the outcome—that is, hypermutation phases 1 and 2, gene conversion or switch recombination—dependent on the way in which the initiating dU/dG lesion is resolved.

Although AID is required for all three programmes of diversification of rearranged immunoglobulin genes[2–7], its mode of action is unknown. The suggestion that AID might act by editing RNA derives from the sequence similarity between AID and Apobec-1 (the catalytic component of the complex that deaminates cytidine 6666 to uracil in the apolipoprotein B messenger RNA, thereby generating a premature stop codon)[1]. But whereas the physiological role of Apobec-1 is to deaminate RNA, the function of AID is to potentiate changes in immunoglobulin gene DNA. It has been suggested that all three programmes of diversification might be initiated by a common type of DNA lesion[8–11], and also that there is a first phase of hypermutation that is specifically targeted to dC/dG pairs[12,13]. These considerations led us to propose the model of immunoglobulin gene diversification shown in Fig. 1.

We visualize diversification as being initiated by AID-mediated deamination of cytidine residues in the immunoglobulin loci. Conventionally this would trigger base-excision repair[14], with uracil being removed by uracil-DNA glycosylase (UDG), followed by cleavage at the abasic site by an apyrimidic endonuclease and reinsertion of a dC residue by a DNA polymerase/deoxyribophosphodiesterase. If instead of being repaired the DNA strand with the dU residue were used as a template for DNA synthesis, then the outcome would be a dC → dT (and a dG → dA) transition (Fig. 1; phase 1A hypermutation). Alternatively, if DNA synthesis were to occur over the abasic site, then both transitions and transversions